

# Dilepton and Photon Emission Rates from a Hadronic Gas II

James V. Steele<sup>1</sup>, Hidenaga Yamagishi<sup>2</sup> and Ismail Zahed<sup>1</sup>

<sup>1</sup>Department of Physics, SUNY, Stony Brook, New York 11794, USA;

<sup>2</sup>4 Chome 11-16-502, Shimomeguro, Meguro, Tokyo, Japan. 153.

(December 2, 2024)

We extend our recent analysis of the dilepton and photon emission rates to the case of finite temperature and baryon density, within the context of a density expansion. To leading order, the effects of the baryon density are assessed using data (photon emission) or constraints from broken chiral symmetry (dilepton emission). Next to leading order effects are worked out, and their contribution qualitatively assessed. The opening of the  $\pi N$  cut causes the photon rate to saturate the empirical photon yield of WA80, but is not enough to fully account for the excess low mass dileptons seen at CERES.

## 1. Introduction

Recent relativistic heavy-ion collisions at CERN have reported an excess of dileptons over a broad range of lepton invariant mass, below the rho mass [1,2]. A possible excess was also reported in the direct photon spectrum [3]. A rate departure from p-A collisions may indicate some medium modifications in the hadronic phase [4], an idea that has spurred considerable attention lately [5–9].

In a recent paper [10] (here after referred to as **I**), we have analyzed the dilepton and photon emission rates from a baryon free hadronic gas using on-shell chiral reduction formulas [11] in the context of a density expansion. At pion density  $n_\pi$  and temperatures of the order of the pion mass  $m_\pi$ , the expansion parameter was identified with  $\kappa_\pi = n_\pi/2m_\pi f_\pi^2 \lesssim 0.3$  [10], where  $f_\pi = 93$  MeV is the pion decay constant. Some enhancement was observed in the low mass dilepton and photon rates due to the “tails” in the vector and axial-vector correlators. This enhancement is however insufficient to account for the empirical excess when inserted in a conventional hydro-evolution of the fire ball, and could be traced back to the detector cuts in transverse momentum [12]. To account for the data, an order of magnitude enhancement in the present bare rate is needed in the low mass region from  $2m_\pi$  to  $4m_\pi$ .

At present CERN energies, both the S-Au and Pb-Au experiments show evidence of a sizable baryonic density in the mid-rapidity region (about two to three times nuclear matter density  $\rho_0$ ). Could it be that such an enhancement is caused by the strong pion-nucleon interactions? Some recent investigations suggest so in the context of some effective models of pion-nucleon dynamics and at specific kinematics (back-to-back emission) [8,9].

In this letter we would like to investigate the role of a finite baryon density in a hadronic gas using the approach

presented in **I**, with an emphasis on constraints brought about by broken chiral symmetry and experiments beyond the threshold region. Specifically, we will use the comprehensive framework introduced in [11] in the form of on-shell chiral reduction formulas. The outcome is a set of general on-shell Ward-identities that could either be saturated by experiment, or approximated near threshold by an on-shell loop-expansion [11,13], and above threshold by resonance saturation [14]. The results conform with the strictures of broken chiral symmetry, relativistic crossing and unitarity. In this sense they are more than conventional dispersion analysis. Both the photon and dilepton rates are subjected to the same analysis due to their common dynamical origin, *albeit* with different kinematics.

In the presence of baryons, we are still able to organize our calculation into a density expansion as was done in **I** for the pions alone. This allows us to separate out the important effects and ascertain the corrections from the higher order terms systematically. In section 2, we outline the character of this density expansion at finite temperature and density. In section 3, we discuss the photon rates, using data and chiral constraints. The effects of nucleons are assessed using a relativistic one-loop chiral expansion without the  $\Delta$  and a chiral expansion with the  $\Delta$  is evaluated in section 4. In section 5, we extend our discussion to the dilepton emission rates to determine the enhancement due to nucleons. We then compute the magnitude of the next to leading order corrections in the density expansion in section 6. Our conclusions are summarized in section 7.

## 2. Dilepton and Photon Rates

In a hadronic gas in thermal equilibrium, the rate **R** of dileptons produced in an unit four volume follows from the thermal expectation value of the electromagnetic current-current correlation function [15]. For massless leptons with momenta  $p_1, p_2$ , the rate per unit invariant momentum  $q = p_1 + p_2$  is given by

$$\frac{d\mathbf{R}}{d^4q} = -\frac{\alpha^2}{6\pi^3 q^2} \mathbf{W}(q) \quad (1)$$

where  $\alpha = e^2/4\pi$  is the fine structure constant,

$$\mathbf{W}(q) = \int d^4x e^{-iq\cdot x} \text{Tr} \left( e^{-(\mathbf{H}-\mu \mathbf{N}-\Omega)/T} \mathbf{J}^\mu(x) \mathbf{J}_\mu(0) \right), \quad (2)$$

$e\mathbf{J}_\mu$  is the hadronic part of the electromagnetic current,  $\mathbf{H}$  is the hadronic Hamiltonian,  $\mu$  the baryon chemical

potential,  $\mathbf{N}$  the baryon number operator,  $\Omega$  the Gibbs energy,  $T$  the temperature, and the trace is over a complete set of hadron states. For leptons with mass  $m_l$ , the right-hand side of (1) is multiplied by

$$(1 + \frac{2m_l^2}{q^2})(1 - \frac{4m_l^2}{q^2})^{\frac{1}{2}}.$$

Similarly, the rate for photons follows from (2) at  $q^2 = 0$ . Specifically,

$$q^0 \frac{d\mathbf{R}}{d^3q} = -\frac{\alpha}{4\pi^2} \mathbf{W}(q) \quad (3)$$

Both (1) and (3) follow from the same current-current correlator (2), albeit for off-shell and on-shell photons respectively. For consistency, both emission rates will be assessed simultaneously as was stressed in **I**.

From the spectral representation and symmetry, the rates may also be expressed in terms of the absorptive part of the time-ordered function

$$\mathbf{W}(q) = \frac{2}{1 + e^{q^0/T}} \text{Im} \mathbf{W}^F(q) \quad (4)$$

$$\mathbf{W}^F(q) = i \int d^4x e^{iq \cdot x} \text{Tr} \left( e^{-(\mathbf{H} - \mu \mathbf{N} - \Omega)/T} T^* \mathbf{J}^\mu(x) \mathbf{J}_\mu(0) \right).$$

We observe that (4) vanishes at  $T = 0$  even for non-zero baryon chemical potential. A cold nuclear state can neither emit real nor virtual photons, for otherwise it would be unstable.

For temperatures  $T \lesssim m_\pi$  and baryonic densities  $n_N \lesssim 3\rho_0$  we may expand the trace in (4) using pion and nucleon states. Expanding the trace in terms of free pions and nucleons, and summing over disconnected pieces lead to the density expansion (see Appendix A)

$$\begin{aligned} -i\mathbf{W}^F(q) &= \langle 0 | \mathcal{O}_J(q) | 0 \rangle_{\text{conn.}} \\ &+ \sum_a \int d\pi \langle \pi | \mathcal{O}_J(q) | \pi \rangle_{\text{conn.}} + \sum_{s,I} \int dN \langle N | \mathcal{O}_J(q) | N \rangle_{\text{conn.}} \\ &+ \frac{1}{2!} \sum_{a,b} \int d\pi_1 d\pi_2 \langle \pi_1 \pi_2 | \mathcal{O}_J(q) | \pi_1 \pi_2 \rangle_{\text{conn.}} \\ &+ \sum_{a,\{s,I\}} \int d\pi dN \langle \pi N | \mathcal{O}_J(q) | \pi N \rangle_{\text{conn.}} \\ &+ \sum_{\{s_1,I_1\},\{s_2,I_2\}} \int dN_1 dN_2 \langle N_1 N_2 | \mathcal{O}_J(q) | N_1 N_2 \rangle_{\text{conn.}} \\ &+ \dots \end{aligned} \quad (5)$$

with the nucleon fields carrying implicit spin and isospin  $N = N^I(p, s)$ , the pion fields implicit isospin  $\pi = \pi^a(k)$ , and

$$\mathcal{O}_J(q) = \int d^4x e^{iq \cdot x} T^* \mathbf{J}^\mu(x) \mathbf{J}_\mu(0).$$

The phase space factors are

$$\begin{aligned} dN &= \frac{d^3p}{(2\pi)^3} \frac{1}{2E_p} \frac{1}{e^{(E_p - \mu)/T} + 1} \\ d\pi &= \frac{d^3k}{(2\pi)^3} \frac{1}{2\omega_k} \frac{1}{e^{\omega_k/T} - 1} \end{aligned}$$

with the nucleon energy  $E_p = \sqrt{m_N^2 + p^2}$  and the pion energy  $\omega_k = \sqrt{m_\pi^2 + k^2}$ . The matrix elements in (5) correspond to the forward scattering amplitudes of a real (photon rate) or virtual (dilepton rate) photon with on-shell nucleons and pions. We consider the nucleons to be in thermal equilibrium and ignore the off-equilibrium effects caused by the collision dynamics on the mid-rapidity nucleons. The chemical potential  $\mu$  is fixed by specifying the nucleon density. We observe that the first term in (5) when used in conjunction with (4) is reminiscent of the resonance gas approximation [16]. The density expansion is an expansion in the number of pions and nucleons in the final state, which means by detailed balance and time-reversal all possible thermal reactions in the initial state.

To leading order in the nucleon and pion densities  $n_N = 4 \int dN 2E_p$  and  $n_\pi = 3 \int d\pi 2\omega_k$  only the first few terms in (5) contribute. A slight refinement is to note that the reduction of one pion is associated with a factor of  $1/f_\pi$ , and that of a nucleon is associated with a factor of  $g_A/f_\pi$ , where  $g_A = 1.26$  is the nucleon axial charge. The dimensionless expansion parameters should be  $\kappa_\pi = n_\pi/2m_\pi f_\pi^2$  and  $\kappa_N = n_N g_A^2/2m_N f_\pi^2$ . For  $T \lesssim m_\pi$  and  $n_N \lesssim 3\rho_0$ , we have  $\kappa_\pi \sim \kappa_N \lesssim 0.3$ . The truncation should be reasonable, unless severe infrared divergences develop. This is unlikely in the hadronic phase since most resonances are massive with finite widths.

### 3. Adding Nucleons

A full treatment of the first two terms of eq. (5) was carried out in **I**. There the electromagnetic current was decomposed into an isovector part  $\mathbf{V}^3$  and an isoscalar part  $\mathbf{B}$ . The  $\mathbf{BB}$  and  $\mathbf{BV}$  correlators are expected to be small in the pionic states, but in the presence of nucleons they must be reassessed. The vacuum contribution is proportional to  $\mathbf{\Pi}_V$ , the transverse part of the vector correlator  $\langle 0 | T^* \mathbf{V} \mathbf{V} | 0 \rangle$  which follows from electroproduction data. Also including terms to first order in the density expansion, we find

$$\begin{aligned} \text{Im} \mathbf{W}^F(q) &= -3q^2 \text{Im} \mathbf{\Pi}_V(q^2) \\ &+ \frac{1}{f_\pi^2} \int d\pi \mathbf{W}_\pi^F(q, k) + \int dN \mathbf{W}_N^F(q, p) \\ &+ \mathcal{O}(\kappa_\pi^2, \kappa_N^2, \kappa_\pi \kappa_N). \end{aligned} \quad (6)$$

The term linear in pion density can be reduced by the use of chiral reduction formulas to a form amenable to experimental determinations. That analysis showed that, to within a few percent, the only important contributions were [10]

$$\begin{aligned}
\mathbf{W}_\pi^F(q, k) &\simeq 12q^2 \text{Im } \mathbf{\Pi}_V(q^2) \\
&- 6(k+q)^2 \text{Im } \mathbf{\Pi}_A((k+q)^2) + (q \rightarrow -q) \\
&+ 8((k \cdot q)^2 - m_\pi^2 q^2) \text{Im } \mathbf{\Pi}_V(q^2) \\
&\times \text{Re}(\Delta_R(k+q) + \Delta_R(k-q))
\end{aligned} \tag{7}$$

with  $\Delta_R(k)$  the retarded pion propagator

$$\Delta_R(k) = \mathbf{P} \mathbf{P} \frac{1}{k^2 - m_\pi^2} - i\pi \text{sgn}(k^0) \delta(k^2 - m_\pi^2),$$

and  $\mathbf{\Pi}_A$  the transverse part of the axial correlator  $\langle 0 | T^* \mathbf{j}_A \mathbf{j}_A | 0 \rangle$  which follows from tau decay data.

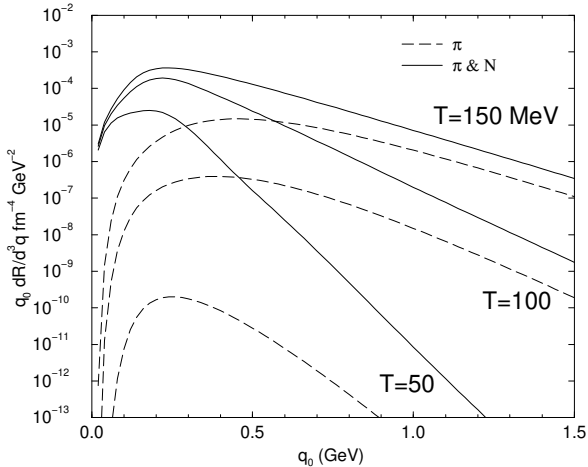


FIG. 1. The photon emission rate to first order in the density expansion for pions only (dashed) and both pions and nucleons (solid). A fixed nucleon density of  $\rho_0$  was used.

Now taking into account the nucleons gives the third term, which is just the spin-averaged forward Compton scattering amplitude on the nucleon with virtual photons. This is only measured for various values of  $q^2 \leq 0$ . However, the dilepton and photon rates require  $q^2 \geq 0$ . Therefore, only the photon rate for this term can be determined directly from data by use of the optical theorem

$$e^2 \mathbf{W}_N^F(q, p) = -4(s - m_N^2) \sum_I \sigma_{\text{tot.}}^{\gamma N}(s) \tag{8}$$

with  $s = (p+q)^2$ . Experimentally, the isospin sum of the cross section in (8) can just be replaced by  $\sigma_{\text{tot.}}^{\gamma d}$  [17] due to the weak collective effect of the two nucleons in the deuteron. The total cross section of  $\gamma d$  is dominated by the  $\Delta(1232)$  [18]. The result for the instantaneous photon rate is shown in fig. 1 for  $T = 50, 100, 150$  MeV and a nucleon density of  $n_N = \rho_0$ . From there it is easy to see that the nucleon contribution dominates over the pions by about an order of magnitude. If the same situation were true for the dilepton rate, the enhancement would probably be enough to explain the excess dileptons in the low-mass region.

This huge correction to the pion result is due to the opening of the  $\Delta$  channel. Approximating the cross section in (8) by a narrow  $\Delta$  resonance, we see the dimensionless parameter of importance is  $(m_\Delta - m_N)/2\Gamma_\Delta \sim 1$  which is multiplied by  $\kappa_N$  under thermal integration. This enhancement from the opening of a new threshold does not iterate in the low mass region. This ensures the density expansion is under control. In section 5 we check whether this enhancement in the photon rate is enough to surpass the upper bound set by WA80 [3].

For off-shell photons, we must resort to chiral constraints to determine the nucleon contribution to the dilepton rate. Broken chiral symmetry dictates uniquely the form of the strong interaction Lagrangian (at tree level) for spin  $\frac{1}{2}$ . Perturbative unitarity follows from an on-shell loop-expansion in  $1/f_\pi$ , that enforces current conservation and crossing symmetry [13].

In general, after summing over spin, only four invariant functions which depend on  $s$  and  $q^2$  remain:

$$\begin{aligned}
\sum_s i \int d^4x e^{iq \cdot x} \langle N_{\text{out}}(p) | T^* \mathbf{J}_\mu(x) \mathbf{J}_\nu(0) | N_{\text{in}}(p) \rangle \\
= 4 (g_{\mu\nu} A + q_\mu q_\nu B + q_{(\mu} p_{\nu)} C + p_\mu p_\nu D).
\end{aligned} \tag{9}$$

The absorptive part, which is of relevance here, only starts to contribute at one-loop. The four invariant functions are related by current conservation — leaving only  $A$  and  $B$  as independent. To one-loop in  $1/f_\pi$  the diagrams that contribute are shown in fig. 2 and require the addition of the crossed diagrams as well. The analytic expressions are quoted in Appendix B for arbitrary  $q^2$ . For on-shell photons, they fulfill the non-renormalization condition  $A(m_N^2, 0) = Z$  with  $Z = 0(1)$  for the neutron (proton). This is fully given by the tree level nucleon contribution, leaving  $A^{\text{loops}}(m_N^2, 0) = 0$  which has been checked to hold analytically for the loop functions.

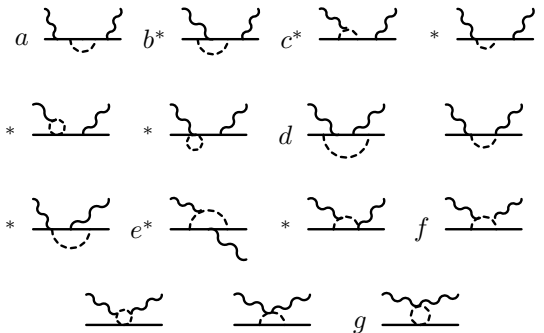


FIG. 2. One-loop diagrams for Compton scattering. The graphs with a star also have a mirror image diagram which must be taken into account and all graphs except for those in the last line require the addition of a crossed diagram. The lettered graphs are discussed in Appendix B.

The results for the photon rate are shown in fig. 3 for a representative temperature  $T = 150$  MeV (results

are similar for other temperatures). Comparison is made with the nucleon result from fig. 1. The one-loop amplitude reproduces the shape attained from the data quite well — even for larger photon energies — with the exception of the small bump around the  $\Delta$  peak. That missing feature, however, is kinematically around the region of interest for the enhancement of the dilepton data (300 MeV above threshold). Therefore to make a full statement about the nucleon contribution for finite  $q^2$ , we will include the  $\Delta$  in the analysis.

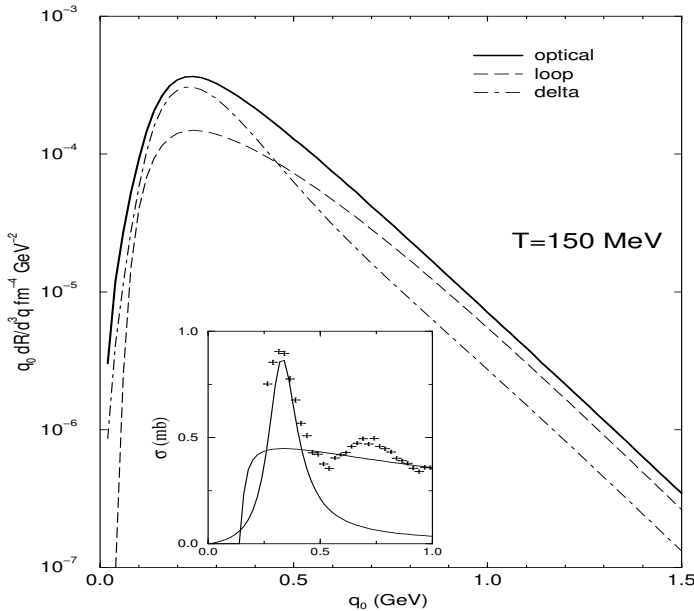


FIG. 3. The photon emission rate as in fig. 1 using data and the optical theorem (solid), using the one-loop results (dashed), and using a contribution from the  $\Delta$  (dashed-dotted). A fixed nucleon density of  $\rho_0$  was used. The inset shows data for  $\sigma_{\text{tot}}^{\gamma d}$  in millibarns as a function of lab momentum in GeV from [17] and the good agreement for the imaginary parts of the one-loop and delta results discussed in the text.

#### 4. The Role of the $\Delta$

Chiral symmetry does not constrain the form of the strong interaction Lagrangian at tree level for spin  $\frac{3}{2}$  in the relativistic approximation. We therefore treat the  $\Delta$  as a resonance in the continuum, and use time reversal invariance and data to constrain the form of the transition matrix element. We decompose the  $N$ - $\Delta$  vector transition matrix element in general as<sup>1</sup>

$$\begin{aligned} \langle N(p) | \mathbf{V}_\mu^a | \Delta(k) \rangle = \bar{u}(p) \left[ & Q(q^2)(\gamma_\mu q_\nu - g_{\mu\nu} \not{q}) \right. \\ & + (R(q^2) + \not{q} \bar{R}(q^2)) (q_\mu q_\nu - g_{\mu\nu} q^2) \\ & \left. + iS(q^2) \sigma_\mu^\lambda q_\lambda q_\nu \right] \gamma_5 u^{\nu,a}(k) \end{aligned} \quad (10)$$

with  $q = k - p$ . Current conservation dictates the specific tensor form of (10). Note that the isoscalar part of the electromagnetic current does not contribute to the nucleon- $\Delta$  transition matrix element.

The modulus square and sum over all spins and isospins of (10) will be denoted by  $\mathcal{M}(k^2, q^2)$  and is quoted in full in Appendix C. It is directly related to the  $\Delta$  contribution of the forward scattering amplitude  $\mathbf{W}_N^F$ ,

$$\mathbf{W}_N^F(q, p) = \text{Im} \frac{4m_N m_\Delta}{s - m_\Delta^2 + im_\Delta \Gamma_\Delta} \mathcal{M}(s, q^2) + (s \rightarrow u)$$

with  $u = (p - q)^2$ . If we were not to take the imaginary part, the full tree level result must also include the nucleon Born terms. At  $q^2 = 0$  this is equal to the isospin sum of  $8A(s, 0)$  and the same non-renormalizability condition of the last section requires  $A^\Delta(m_N^2, 0) = 0$ . This is satisfied trivially by the decomposition used in eq. (10), since the charge was fixed to zero by current conservation.

If we do not contract the vector indices of  $\mathbf{W}_N^F$  as in eq. (9), we can also determine  $B(s, q^2)$ . The polarizabilities are defined as

$$\begin{aligned} \bar{\alpha} + \bar{\beta} &= -2\alpha m_N A''(m_N^2, 0) = \frac{8\alpha}{9} \frac{m_N^2 m_\Delta^2 + m_N^2}{m_\Delta^2 m_\Delta^2 - m_N^2} Q^2 \\ \bar{\beta} &= -\frac{\alpha}{m_N} B(m_N^2, 0) = \frac{8\alpha}{9} \frac{Q^2}{m_\Delta - m_N}, \end{aligned}$$

over-constraining the value of  $Q$ . Although experiment has shown the electric polarizability dominates over the magnetic one  $\bar{\alpha} > \bar{\beta}$ , the  $\Delta$  is a magnetic dipole effect and tends to overestimate  $\bar{\beta}$  in other calculations [19]. Therefore we concentrate on fixing a reasonable value for  $\bar{\alpha} + \bar{\beta} = 10 \times 10^{-4} \text{ fm}^3$ . This indeed gives a  $\bar{\beta} \simeq 14 \times 10^{-4} \text{ fm}^3$  about three times the experimental value. This corresponds to  $Q(0) = 2.75/m_N$ . Translating into our notation, it is comparable to the value  $Q \simeq 2.5/m_N$  obtained by a different method [20].

The decay width of the  $\Delta$  is given by

$$\Gamma_{\Delta \rightarrow N\gamma} = \alpha m_N \frac{m_\Delta^2 - m_N^2}{8m_\Delta^2} \mathcal{M}(m_\Delta^2, 0) \simeq 0.72 \text{ MeV},$$

and can be used to fix  $S(0) = 1.2/m_N^2$ . This compares well with  $S \simeq 1.0/m_N^2$  from [20].

The form factors  $R, \bar{R}$  do not contribute at  $q^2 = 0$ . For finite  $q^2$ , the  $\Delta$  contribution is mostly around its mass shell and so we can use the Dirac equation to rewrite

<sup>1</sup>We could also include terms with  $\gamma_\mu u^\mu$ , but these are suppressed near the mass-shell, where we are interested.

$\not{q}\not{R} \rightarrow (m_\Delta + m_N)\not{R}$  in (10) and absorb  $\not{R}$  into the definition of  $R$ . Then using the vertex (10) in pion electro-production,  $R$  can be shown to be proportional to the longitudinal part of the cross section. This is on the order of 10% of the total result even for moderate  $q^2$  and therefore we will take  $R = \not{R} = 0$  for the rest of this paper.

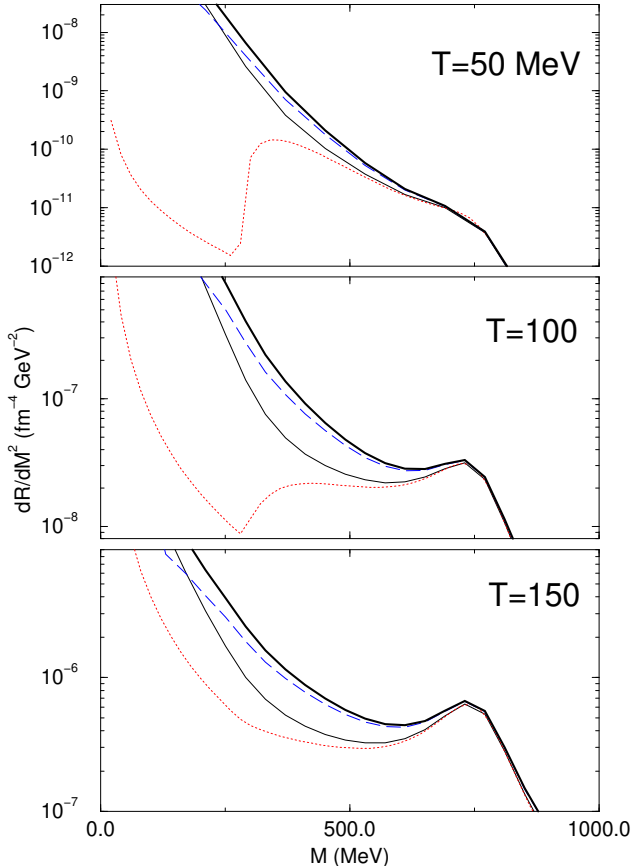


FIG. 4. The dielectron rate for pions alone (dotted), pions and  $\Delta$  (solid), and pions and one-loop (dashed). The contribution from pions,  $\Delta$ , and one-loop together is represented by the thick solid line. A fixed nucleon density of  $\rho_0$  was used.

We plot the photon rate due to the  $\Delta$  along with the one-loop result in fig. 3. From there we see that the  $\Delta$  rate does quite well around the peak and then dies away for larger energies. In fact, adding the one-loop and  $\Delta$  rates, we come very close to reproducing the nucleon result obtained from the data. This even includes the secondary peak, seen in the inset of fig. 3, which is fit moderately well by the loop contribution. Therefore we take both contributions into account as a way to parameterize the photon spectral function with on-shell chiral symmetry, relativistic crossing, and unitarity constraining the function near threshold, and experiment constraining it above. We now can move to finite  $q^2$  to ascertain the dilepton rate.

## 5. Dilepton Rates with Nucleons

We will neglect the momentum dependence of the form factors in eq. (10) since they are expected to be of monopole form  $(1 - q^2/4M_+^2)^{-1}$  with  $M_+ = \frac{1}{2}(m_N + m_\Delta)$  [21] and hardly change for the  $q^2$  we will examine (less than 1 GeV $^2$ ). Then taking the results of the previous section to  $q^2 > 0$  gives the curves in fig. 4. Also shown is the one-loop result and the pion result from **I** for comparison.

Qualitatively, the rates are similar to the photon case. The enhanced bump of the  $\Delta$  is smeared out and enhances the rate by as much as a factor of ten (for  $T = 100$  MeV) before gradually dying out again near the  $\rho$  peak. The tail of the one-loop goes above the  $\Delta$  result around  $M = 200$  MeV. This may be easily understood by noting that the absorptive part involves the  $\pi N$  cut, with pions typically carrying a momentum of order  $m_\pi$  and the nucleon a momentum of order  $p_F \sim m_\pi$ . The one-loop is also overtaken by the pion result at the  $\rho$  peak. A closer examination of the one-loop real part shows that it is about half of the tree result for  $q^2 \gtrsim (300\text{MeV})^2$ , above which the  $1/f_\pi$  expansion is no longer reliable. Fortunately, the energetic dilepton pairs with  $q^0 \gtrsim 300$  MeV are thermally suppressed by almost an order of magnitude at the highest temperature, typically  $e^{-300/150} \sim 1/7$ .

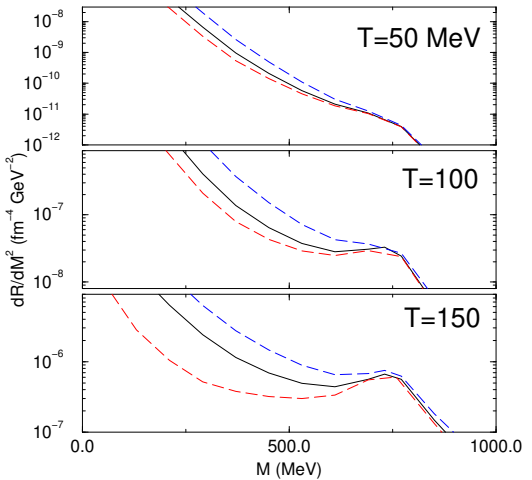


FIG. 5. The dielectron rate including the pions,  $\Delta$ , and one-loop for  $\rho_0$  (solid),  $\frac{1}{2}\rho_0$  (lower dashed), and  $3\rho_0$  (upper dashed).

Combining the one-loop and  $\Delta$  results gives the thick solid line in fig. 4. The dominant effect in our case comes from the continuum and not the  $\Delta$  resonance. At  $M = 400$  MeV, the inclusion of nucleons enhances the rate by a factor of three. Others who have taken nucleons into account through various methods [5,8,9] find enhancements in the rate similar to our result. However, the details of the in-medium effects are not needed in this

analysis and so should be considered more general. Also in our calculations there is no shift of the dilepton pair production  $\rho$  peak.

In fig. 5 we show the dependence of the  $T = 150$  MeV dielectron rate on the nucleon density for  $n_N = \frac{1}{2}\rho_0, \rho_0$ , and  $3\rho_0$ . At  $T = 150$  MeV and  $\frac{1}{2}\rho_0$ , the result is dominated by the pions as the nucleon contribution is extremely small. This shows the effect is truly from the nucleon density. Even so, only at  $3\rho_0$  does the rate flatten out at the value of the  $\rho$  peak rather than increasing towards it.

In order to fully understand the role of the cuts, we follow [8] and evolve the instantaneous rate over space-time using recent transport equation results [5] and experimental cuts [1]. Assuming a homogeneous expansion, the volume and temperature only depend on time and can be parameterized as

$$V(t) = V_0 \left(1 + \frac{t}{t_0}\right)^3 \quad T(t) = (T_i - T_\infty) e^{-t/\tau} + T_\infty$$

with  $t_0 = 10(10.8)$  fm/c and  $\tau = 8(10)$  fm/c for S-Au (Pb-Au) collisions. The freeze-out time is  $t_{\text{f.o.}} = 10(20)$  fm/c. We absorb  $V_0$  into an overall normalization constant that includes the charged particle distribution as well. RQMD predicts the initial baryon density  $n_B \simeq 2.5\rho_0$  for S-Au and  $4\rho_0$  for Pb-Au [22] which translates into  $n_N \simeq 0.7\rho_0(1.0\rho_0)$ . Only the pion and nucleon densities are retained since we are expanding the emission rates (5) in terms of *stable* final states, summing over all possible initial states. This point is particularly transparent in the  $\rho$  region. Assuming chemical equilibrium gives a constant nucleon chemical potential. The rate then can be written as

$$\frac{(dN/d\eta dM)}{(dN_{ch}/d\eta)} = N_0 M \int_0^{t_{\text{f.o.}}} dt V(t) \int \frac{d^3 q}{q_0} A(q^0, q^2) \frac{d\mathbf{R}}{d^4 q}$$

with the normalization constant  $N_0 = 6.76(1.33) \times 10^{-7}$  fixed by the transport results in [5]. The acceptance function  $A$  ensures the detector cuts at CERES ( $p_\perp > 200(175)$  MeV,  $2.1 < \eta < 2.65$ , and  $\Theta_{ee} > 35$  mrad) are taken into account. The finite mass resolution is also taken into account by folding the spectrum with a Gaussian averaging function given by the CERES collaboration [12].

Finally, we plot the results for S-Au and Pb-Au collisions in fig. 6. This requires the addition of the Dalitz and omega decays which were obtained from the transport model [5]. The data is presented by adding the statistical and systematic errors linearly. The Pb-Au data is still preliminary. For  $n_N = 0$ , the pion result alone has already been analyzed in two hydro-dynamical models [12,6]. Comparison of this alone can be used to test the validity of the evolution in space-time described above. Our result is shown as the dashed line in fig. 6. The overall shape due to the cut looks reasonable. The values for the rate in [12] are an order of magnitude smaller, but

this can be traced back to a shorter time in the hadronic phase. The agreement with [6] are fair. We can think of the results of this space-time evolution as an upper bound on the results from a true hydro-dynamical model.

Adding the nucleon contribution gives the solid line in fig. 6. The effect of the cuts is dramatic, resulting in a very small enhancement. Only if we take the extreme case of the baryon density totally saturated by nucleons do we start to reach the lower error bars of the data in the  $M = 200 - 400$  MeV regime as shown by the dashed-dotted line. The large effect seen in fig. 4 is not present because the temperature dies away quickly, thereby decreasing the nucleon density and rate dramatically as seen in fig. 5.

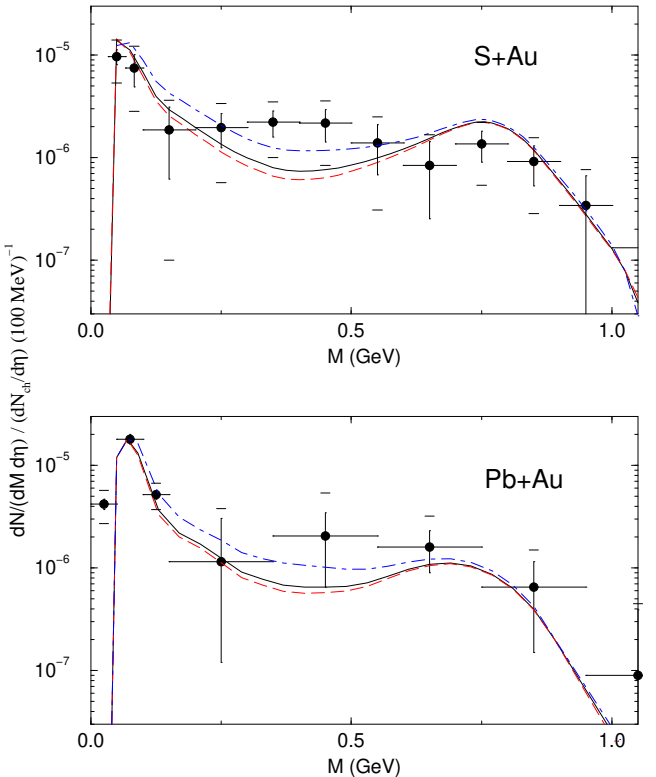


FIG. 6. Our dielectron rate including the  $\Delta$  and one-loop contributions evolved in space-time as in [8] for S-Au and Pb-Au collisions. In the upper graph,  $n_N = 0, 0.7\rho_0$ , and  $2.5\rho_0$  are plotted as the dashed, solid, and dashed-dotted lines respectively. In the lower graph, the lines are for  $n_N = 0, 1.0\rho_0$ , and  $4\rho_0$ . The data are from [1]. The systematic errors are added linearly to the statistical error bars to give the cross line. The Pb-Au data is preliminary.

Comparing to [8], our rate is slightly smaller in the region of interest. This can be traced back to the bare rates. For  $M \gtrsim 400$  MeV, their rate for  $n_N = 0.5\rho_0$  is *larger* than the rate for  $n_N = \rho_0$  [23] which differs from our result in which the nucleon contribution dies away continuously leaving only the pion contribution (fig. 5).

This is related to the depletion of the  $\rho$  peak in [8], which does not occur in our case.

We can also evolve the photon rates and compare with the upper bounds set by WA80 for S-Au [3]. The procedure is similar to that for the dileptons above. The acceptance cut is  $2.1 \leq \eta \leq 2.9$  and no integration over momentum is required. In this case the factor  $N_0$  is only the volume  $V_0$  which we normalize by comparison with [12] for  $n_N = 0$ . This fixes  $V_0 \simeq 300 \text{ fm}^3$  which corresponds to an initial radius of 4 fm and agrees with central collision estimates. The result for the pion (dashed line) and full result (solid line) are shown in fig. 7. The inclusion of nucleons put the rate right on the edge of the upper limit for the data. Since we have analyzed both the dilepton and photon rates simultaneously, this implies that more enhancement of the dilepton rate would overshoot the photon data, a particularly important point in our analysis.

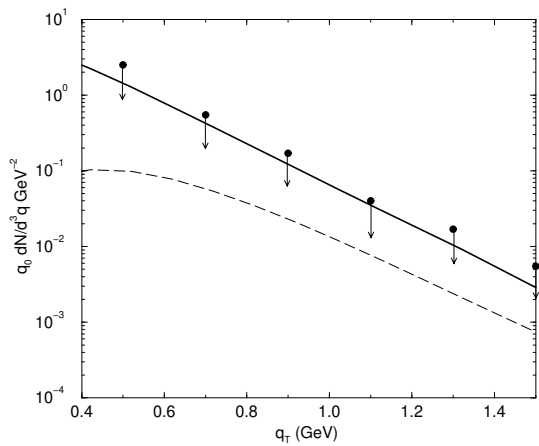


FIG. 7. Our photon rate with (solid) and without (dashed) the nucleon contribution discussed in this paper. The data are upper bounds from [3].

## 6. Higher Order Terms

We have now assessed all the terms of eq. (5) linear in the density. The result is that they cannot explain the CERES data. In general, higher order terms will be suppressed by more powers of the expansion parameter. Since we have a consistent density expansion, this implies the inclusion of higher order effects will not be dramatic. However, this rule of thumb can be upset if new thresholds open up in the low mass region. Pulling the second order terms out of eq. (6), we have

$$\begin{aligned} \delta \text{Im } \mathbf{W}^F(q) &= \frac{1}{2f_\pi^4} \int d\pi_1 d\pi_2 \mathbf{W}_{\pi\pi}^F(q, k_1, k_2) \\ &+ \frac{1}{f_\pi^2} \int d\pi dN \mathbf{W}_{\pi N}^F(q, k, p) \end{aligned}$$

$$+ \int dN_1 dN_2 \mathbf{W}_{NN}^F(q, p_1, p_2) + \mathcal{O}(\kappa^3). \quad (11)$$

Note that matrix elements involving nucleons carry an implicit factor of  $1/f_\pi^2$  since the contribution only starts at one-loop. Experimentally, we can estimate the strength of the third term in eq. (11) at  $q^2 = 0$  as follows. We noted in connection with eq. (8) in the last section that the cross section for Compton scattering on a deuteron is identical to the sum of Compton scattering on a proton and neutron individually. This seems to indicate that the collective effect of two nucleons is small and we will ignore it for the rest of this paper.

The  $\Delta$  may be thought of as a bound state of a pion and a nucleon, and so the second term in eq. (11) could be important. We also must retain the isoscalar contribution  $\mathbf{B}_\mu$  to the electromagnetic current when nucleons are involved. We can still reduce out the pions as given in [11] if we assume the pions do not interact with the isoscalar part. This is true in the soft pion limit and so should be a good approximation [10]. The overall form of  $\mathbf{W}_{\pi N}^F$  is very similar to  $\mathbf{W}_\pi^F$ , in which one pion was also reduced out, with the vacuum matrix elements being replaced by averages in a nucleon state. The result is

$$\begin{aligned} \mathbf{W}_{\pi N}^F(q, k, p) &= -4 \text{Im } i \sum_{s, I} \int d^4x e^{iq \cdot x} \\ &\times \langle N_{\text{out}}(p) | T^* \mathbf{J}_\mu(x) \mathbf{J}^\mu(0) - \mathbf{B}_\mu(x) \mathbf{B}^\mu(0) | N_{\text{in}}(p) \rangle \\ &+ \sum_{a, \{s, I\}} \epsilon^{a3g} \epsilon^{a3f} \\ &\times \text{Im} \left( g^{\mu\nu} - (k+q)^\mu (2k+q)^\nu \Delta_R(k+q) \right. \\ &\quad \left. + (k+q)^\mu (k+q)^\nu (2k+q)^2 \Delta_R^2(k+q) \right) \\ &\times \int d^4x e^{i(k+q) \cdot x} \langle N_{\text{out}}(p) | T^* \mathbf{j}_{A\mu}^f(x) \mathbf{j}_{A\nu}^g(0) | N_{\text{in}}(p) \rangle \\ &+ (q \rightarrow -q) \\ &+ 8k^\mu k^\nu \text{Im } i \sum_{s, I} \int d^4x e^{iq \cdot x} \\ &\times \text{Re} (\Delta_R(k+q) + \Delta_R(k-q)) \\ &\times \langle N_{\text{out}}(p) | T^* \mathbf{J}_\mu(x) \mathbf{J}_\nu(0) - \mathbf{B}_\mu(x) \mathbf{B}_\nu(0) | N_{\text{in}}(p) \rangle \\ &+ 3m_\pi^2 f_\pi \int d^4x d^4y e^{iq \cdot (x-y)} \\ &\times \sum_{s, I} \text{Im} \langle N_{\text{out}}(p) | T^* \mathbf{J}_\mu(x) \mathbf{J}^\mu(y) \hat{\sigma}(0) | N_{\text{in}}(p) \rangle \\ &- k^\alpha k^\beta \int d^4x d^4y d^4z e^{iq \cdot (x-y)} e^{-ik \cdot z} \\ &\times \text{Im } i \langle N_{\text{out}}(p) | T^* \mathbf{J}_\mu(x) \mathbf{J}^\mu(y) \mathbf{j}_{A\alpha}^a(z) \mathbf{j}_{A\beta}^a(0) | N_{\text{in}}(p) \rangle \\ &+ k^\beta \text{Im} (\delta_\mu^\alpha - (2k+q)_\mu (k+q)^\alpha \Delta_R(k+q)) \\ &\times \int d^4x d^4y e^{ik \cdot (y-x)} e^{-iq \cdot x} \end{aligned}$$

$$\times \sum_{a, \{s, I\}} i\epsilon^{a3e} \langle N_{\text{out}}(p) | T^* \mathbf{j}_{A\alpha}^e(x) \mathbf{j}_{A\beta}^a(y) \mathbf{J}^\mu(0) | N_{\text{in}}(p) \rangle \\ + (q \rightarrow -q) + (k \rightarrow -k) + (q, k \rightarrow -q, -k)$$

with  $\tilde{\mathbf{\Pi}}_A$  denoting the transverse part of  $\langle N | T^* \mathbf{j}_A \mathbf{j}_A | N \rangle$  summed over spin and isospin. We use the same analysis as the last section for the  $\mathbf{JJ}$  term. The contribution here is negative, but weighted by an extra factor of  $\kappa$ . It is about 10% of the leading contribution. Since there is no prominent resonance with the quantum numbers of the isoscalar term  $\mathbf{BB}$ , the imaginary part should also be small and will be neglected.

The second term contains the axial current  $\mathbf{j}_A$ , which is a pionic contribution, and so this term may feed into the  $\Delta$ . Using the decomposition ( $k = p' - p$ )

$$\langle N(p) | \mathbf{j}_{A\mu}^a | \Delta(p') \rangle = \bar{u}(p) \left[ F(k^2) g_{\mu\nu} + G(k^2) \gamma_\mu k_\nu \right. \\ \left. + H(k^2) k_\mu k_\nu + iI(k^2) \sigma_\mu^\lambda k_\lambda k_\nu \right] u^{\nu, a}(p')$$

an analysis of  $\pi N$  scattering in [24] showed that  $F(0) = 1.38$  and  $G(0) = 0.4/m_N$ . Using the fact that  $H$  and  $I$  are suppressed for large  $N_c$ , we can justify keeping only the  $F$  term to find

$$\int d^4x e^{iK \cdot x} i \langle N_{\text{out}}(p) | T^* \mathbf{j}_{A\mu}^f(x) \mathbf{j}_{A\nu}^g(0) | N_{\text{in}}(p) \rangle = \\ = -\frac{32F^2}{9} \delta^{fg} \frac{p \cdot K + m_N(m_N + m_\Delta)}{(p + K)^2 - m_\Delta^2 + im_\Delta \Gamma_\Delta} \\ \times \left( g_{\mu\nu} - \frac{(p + K)_\mu (p + K)_\nu}{m_\Delta^2} \right) + (K \rightarrow -K)$$

where only the  $\Delta$  channel has been retained. This term and its crossed counterpart gives a positive contribution to the rate. Numerical results show this term is appreciable right near threshold but quickly shrinks to 10% of the terms linear in  $\kappa$  and practically vanishes even before the  $\Delta$  peak is reached. The damping is simply coming from the exponential factors in phase space and so the only place where this term is significant is within the Dalitz tail. This behavior is expected to occur for all terms in  $\mathbf{W}_{\pi N}^N$  and so we may neglect the terms of order  $\kappa_N \kappa_\pi$ .

For completeness, we quote the result for the first term in (11) in Appendix D. Qualitatively, we note that the full  $\pi\pi$  scattering amplitude as well as terms of photon-pion scattering similar to  $\mathbf{W}_\pi$  appear with an additional suppression factor of  $\kappa$ . In the soft pion limit most of the correlation functions in the pionic state are amenable to correlations in the vacuum, some of which were assessed in **I** and found to be small. Hence, we expect qualitatively that  $\mathbf{W}_{\pi\pi}^F$  is suppressed by the factor  $\kappa_\pi^2$  as expected and hence are small in comparison with the lower order terms.

## 7. Conclusions

We have extended the analysis in **I** to account for possible nucleon densities in assessing the photon and emission rates from a hot hadronic gas. We have used the very general framework put forward in [11,14,13] to allow for a comprehensive analysis of the emission rates in powers of the matter densities, and enforce the known constraints of broken chiral symmetry on-shell, current conservation, and relativistic unitarity. We believe that most approaches to this problem as well others involving issues of chiral symmetry in matter, have to embody the chiral Ward-identities established on-shell in [11], whether at threshold or above.

Our purpose of this paper was to use these arguments in combination with a density expansion to account for a systematic analysis of the dilepton and photon rates from a hot hadronic gas at finite nucleon density. For the photon rate, we have used the constraints from broken chiral symmetry and data to leading order in the densities. A large enhancement of photons in the low energy region was found. Using an on-shell expansion to one-loop and a general decomposition of the  $\Delta$ , we were able to reproduce the photon rates at  $q^2 = 0$ .

We have used the same amplitude to estimate the dilepton production rate at  $q^2 > 0$ . In the latter, we have found an enhancement from the  $\pi N$  cut in the low mass region for a nucleon density on the order of nuclear matter density on top of the already large enhancement from thermal reactions *alone*. This enhancement is caused by the opening of a threshold in the  $\pi N$  channel, and does not iterate coherently in the next order corrections, which we have found to be qualitatively small and mostly confined to the Dalitz region.

For S-Au and Pb-Au reactions, we have evolved the dilepton rate in space-time and taken the experimental cuts. The result is insufficient to explain the data, and this even with some liberal choices of the parameters. The nucleon densities do trigger large dilepton yields but die out quickly after short reaction times. In addition, we have evolved the photon rates and found the results on the edge of the upper bounds of the data. This means that any further enhancement would overshoot the empirical measurements. Since we have a consistent and controlled expansion scheme, these results lead us to suspect the nucleons cannot explain the data. Any mechanism which could explain the data would need to have a very specific form in order not to upset the photon yield. However, this space-time evolution is still only a qualitative assessment. Quantitative results from a full hydrodynamical model which takes into account the quark-gluon phase, flow, and hadronic multiplicities is needed for a final analysis.

Our results imply a different interpretation for the role of the nucleons compared with a number of recent estimates [8,9,25]. Our analysis, however, is different in a number of ways. We have evaluated the rates at finite temperature, since there is no emission in cold matter.

Also our results go smoothly into those of **I** at zero nucleon density, thereby enforcing the known constraints of (on-shell) broken chiral symmetry, current conservation, relativistic crossing and unitarity for all dilepton kinematics. It is important to stress that our density expansion is an expansion in the number of pions and nucleons in the final state, which means by detailed balance and time-reversal all possible thermal reactions in the initial state. Finally, our qualitative assessment of the next to leading order shows that the expansion is reliable in the low mass region, with no apparent need for coherent resummations.

The empirical consequence of these differences is that the dilepton strength in the  $\rho$  region from a hot hadronic gas remains about constant and dominated by thermal  $\pi\pi$  pairs. The enhancement below this region in invariant mass does not come at the expense of this peak. A consequence of this is the enhancement is very sensitive to the temperature and nucleon density and dies away quickly as the fireball evolves. The resolution in the  $\rho$  region for the CERES data is not enough to sort out the dilepton emission from ‘cold’  $\omega$ ’s. An improvement on this resolution maybe an important step in assessing the effects of interaction as reported here in comparison to those discussed in [5,8,9,25]. Another improvement, as stressed in **I**, is to have more empirical correlations between the photon and dilepton yields.

### Acknowledgements

We would like to thank G.E. Brown, G.Q. Li, M. Prakash, E.V. Shuryak, and H. Sorge for discussions. We especially thank R. Rapp for discussion and supplying us with the details of his calculation. This work was supported in part by the US DOE grant DE-FG02-88ER40388.

### Appendix A

Denoting momentum and isospin as one discretized variable  $k$  for compact notation, a general term in the pion density expansion for any operator  $\mathcal{O}$  is

$$\frac{1}{N!} \sum_{\{n_i, k_i\}} \langle \Pi_N | e^{-(H-F)/T} \mathcal{O} | \Pi_N \rangle_{\text{conn.}}$$

with  $\Pi_N = n_1 \pi_{k_1} \dots n_N \pi_{k_N}$  and the  $1/N!$  added for proper normalization. For  $N = 1$ , the one-pion connected piece is

$$\sum_{n,k} n e^{-(n\omega-F)/T} \langle \pi_k | \mathcal{O} | \pi_k \rangle_{\text{conn.}} = \sum_k n_B(\omega) \langle \pi_k | \mathcal{O} | \pi_k \rangle_{\text{conn.}}$$

with  $n_B(\omega) = (e^{\omega/T} - 1)^{-1}$  the Bose-Einstein momentum distribution. The two-pion connected piece is

$$\frac{1}{2!} \sum_{n,k} \frac{n(n-1)}{2!} e^{-(n\omega-F)/T} \langle \pi_k \pi_k | \mathcal{O} | \pi_k \pi_k \rangle_{\text{conn.}}$$

$$= \frac{1}{2!} \sum_k (n_B(\omega))^2 \langle \pi_k \pi_k | \mathcal{O} | \pi_k \pi_k \rangle_{\text{conn.}}$$

Now for  $N = 2$ , the pions must have different quantum numbers in order not to double count and leads to

$$\frac{1}{2!} \sum_{k_1 \neq k_2} n_B(\omega_1) n_B(\omega_2) \langle \pi_{k_1} \pi_{k_2} | \mathcal{O} | \pi_{k_1} \pi_{k_2} \rangle_{\text{conn.}}$$

and so combining the two-pion pieces from  $N = 1$  and  $N = 2$ , we have the sum over non-restricted momentum for the two pions. This generalizes for higher number of particles. A similar argument holds for fermions with finite chemical potential by replacing  $n_B(\omega)$  by the Fermi distribution.

### Appendix B

The on-shell one-loop result can be written in terms of Feynman parameter integrals. Since we are only considering the imaginary parts, the (real) subtraction constants will be ignored.

$$\begin{aligned} f_\pi^2 A(s, q^2) = & Z(g_A^2 - 1) \left( 1 - \frac{q^2}{s - m_N^2} \right) J_{22}^{\pi\pi}(q^2) \\ & - 4m_N(g_A \tilde{G} + \sigma_{\pi N}) \overline{\Gamma}_3^{\pi\pi}(q^2) \\ & + Z \frac{q^2 G^2}{s - m_N^2} \left[ 2\Gamma_3^{\pi N}(s) - J^{NN}(q^2) - 4\Gamma_3^{N\pi}(s) \right. \\ & \left. + \frac{3}{2} J_1^{\pi N}(s) - m_\pi^2 \Gamma^{\pi N}(s) \right] \\ & - 3Z^2 G^2 \frac{4q^2 m_N^2}{(s - m_N^2)^2} [J^{\pi N}(s) - J_1^{\pi N}(s)] \\ & + 4G^2 [\Gamma_3^{\pi\pi}(q^2) - \Gamma_3^{NN}(q^2)] + G^2 J^{NN}(q^2) \\ & + \frac{1}{2} ZG^2 [4\Gamma_3^{NN}(q^2) - J^{NN}(q^2) - 3J_1^{\pi N}(s)] \\ & + G^2 \left( 1 - \frac{3}{2} Z \right) (s - m_N^2) \Gamma^{\pi N}(s) \\ & + 2ZG^2 (s - m_N^2) \Gamma_1^{\pi N}(s) + 2ZG^2 q^2 \Gamma_2^{\pi N}(s) \\ & + (Z-2)2m_\pi^2 G^2 \mathcal{G}_4^{\pi N} + (Z-1)4m_\pi^2 G^2 \Omega_4 \\ & - 4m_\pi^2 G^2 \mathcal{G}_4^{N\pi} + \frac{1}{2}(Z-2)G^2 q^2 [m_\pi^2 \mathcal{G}^{\pi N} + 2\Gamma_{12}^{NN}(q^2)] \\ & + \text{crossed} \end{aligned}$$

$$\begin{aligned} f_\pi^2 B(s, q^2) = & -4 (m_N \sigma_{\pi N} - (g_A m_N - G)^2) \\ & \times \left[ \Gamma_{456}^{\pi\pi}(q^2) - \Gamma_{12}^{\pi\pi}(q^2) + \frac{1}{4} \Gamma^{\pi\pi}(q^2) \right] \\ & + ZG^2 \frac{4m_N^2}{s - m_N^2} \left[ 2\Gamma_4^{\pi N}(s) + 2\Gamma_5^{\pi N}(s) - \Gamma^{N\pi}(s) \right. \\ & \left. + 4\Gamma_1^{N\pi}(s) + 2\Gamma_2^{N\pi}(s) - 4\Gamma_4^{N\pi}(s) - 4\Gamma_5^{N\pi}(s) \right] \end{aligned}$$

$$\begin{aligned}
& + 2(Z-2)G^2 [\Gamma_{456}^{NN}(q^2) - \Gamma_{12}^{NN}(q^2)] \\
& + 2ZG^2\Gamma_{456}^{\pi N}(s) - 2G^2\Gamma_{12}^{\pi N}(s) - G^2 [\Gamma^{N\pi}(s) - 2\Gamma_{12}^{N\pi}(s)] \\
& - 2ZG^2 [2\Gamma_{456}^{N\pi}(s) - \Gamma_{12}^{N\pi}(s)] \\
& + 2(Z-2)m_\pi^2 G^2 [\mathcal{G}_{10}^{\pi N} - \mathcal{G}_3^{\pi N}] + 4(Z-1)m_\pi^2 G^2 \Omega_5 \\
& - 4m_\pi^2 G^2 \left[ \mathcal{G}_{10}^{N\pi} - \mathcal{G}_3^{N\pi} + \frac{1}{4}\mathcal{G}^{N\pi} \right] \\
& + \text{crossed}
\end{aligned}$$

$$C = \frac{2}{q^2 + m_N^2 - s} (A + q^2 B) \quad D = \frac{2q^2}{q^2 + m_N^2 - s} C$$

with  $\Gamma_{456} = \Gamma_4 + 2\Gamma_5 + \Gamma_6$  and  $\Gamma_{12} = \Gamma_1 + \Gamma_2$ . Also  $g_A$  is the nucleon axial charge,  $\sigma_{\pi N}$  is the pion-nucleon sigma term,  $G = f_\pi g_{\pi NN}$ , and  $\bar{G} = 2G - g_A m_N$ . The values used were  $g_A = 1.26$ ,  $m_N = 940$  MeV,  $m_\pi = 140$  MeV, and  $\sigma_{\pi N} = 45$  MeV to ensure the nucleon is on-shell. Taking  $q^2 = 0$  and  $\sigma_{\pi N} \rightarrow 0$  reduces the loop result to that given in [19]. Conformity with the Ward-identities [11] requires an on-shell expansion [13] as taken into account here.

Each of the  $J$ ,  $\Gamma$ ,  $\mathcal{G}$  and  $\Omega$ 's are Feynman parameterization integrals quoted in full in [13]. The imaginary parts have cuts for  $s > s_0 = (m_N + m_\pi)^2$  and  $q^2 > 4m_\pi^2$ . The cuts for  $q^2 > 4m_N^2$  do not impact this paper and are not quoted, thereby making the contributions from  $J^{NN}$  and  $\Gamma_i^{NN}$  zero. The labeled diagrams in fig. 2a-h are dominated by  $J^{\pi N}$ ,  $\Gamma^{\pi N}$ ,  $\Gamma^{N\pi}$ ,  $\mathcal{G}^{\pi N}$ ,  $\Omega$ ,  $\mathcal{G}^{N\pi}$ ,  $\Gamma^{\pi\pi}$ , and  $J^{\pi\pi}$  respectively (fully given by these if the  $\pi N$  coupling were a constant rather than proportional to a derivative in the Lagrangian).

We only need to quote a subset of the integrals and obtain the others by use of algebraic manipulations as outlined in [19]. Using  $\lambda(x, y, z) = x^2 + y^2 + z^2 - 2xy - 2xz - 2yz$ ,  $\lambda_\pi = \lambda(s, m_N^2, m_\pi^2)$ ,  $\lambda_q = \lambda(s, m_N^2, q^2)$ , and  $\lambda_{\pi q} = \lambda(q^2, m_\pi^2, m_\pi^2)$ , the imaginary parts for  $q^2 \geq 0$  are

$$\begin{aligned}
\text{Im } J^{\pi\pi}(q^2) &= \frac{\sqrt{\lambda_{\pi q}}}{16\pi q^2} \theta(q^2 - 4m_\pi^2) \\
\text{Im } J^{\pi N}(s) &= \frac{\sqrt{\lambda_\pi}}{16\pi s} \theta(s - s_0) \\
\text{Im } \Gamma^{\pi\pi}(q^2) &= \frac{1}{16\pi \lambda_{\pi q}} \theta(q^2 - 4m_\pi^2) \\
\text{Im } \Gamma^{\pi N}(s) &= -\frac{1}{16\pi \sqrt{\lambda_q}} \ln \left[ \frac{a_{\pi q} + \sqrt{\lambda_\pi \lambda_q}}{a_{\pi q} - \sqrt{\lambda_\pi \lambda_q}} \right] \theta(s - s_0) \\
\text{Im } \Gamma^{N\pi}(s) &= -\frac{1}{16\pi \sqrt{\lambda_q}} \ln \left[ \frac{b_{\pi q} + \sqrt{\lambda_\pi \lambda_q}}{b_{\pi q} - \sqrt{\lambda_\pi \lambda_q}} \right] \theta(s - s_0) \\
& + \frac{1}{16\pi \sqrt{\lambda_q}} \ln \left[ \frac{c_{\pi q} + \sqrt{\lambda_\pi \lambda_q}}{c_{\pi q} - \sqrt{\lambda_\pi \lambda_q}} \right] \theta(q^2 - 4m_\pi^2) \\
\text{Im } \mathcal{G}^{\pi N} &= \frac{\sqrt{\lambda_\pi}}{4\pi} \frac{s}{a_{\pi q}^2 - \lambda_\pi \lambda_q} \theta(s - s_0) \\
\text{Im } \mathcal{G}^{N\pi} &= \frac{\sqrt{\lambda_\pi}}{4\pi} \frac{s}{b_{\pi q}^2 - \lambda_\pi \lambda_q} \theta(s - s_0)
\end{aligned}$$

$$\begin{aligned}
& - \frac{1}{8\pi q^4} \frac{\sqrt{\lambda_{\pi q}}}{s - m_N^2 + m_\pi^2} \theta(q^2 - 4m_\pi^2) \\
\text{Im } \Omega &= \frac{1}{16\pi \sqrt{\lambda_q} (s - m_N^2 - q^2)} \theta(s - s_0) \\
& \times \left\{ \ln \left[ \frac{e_{\pi q} + \sqrt{\lambda_\pi \lambda_q}}{e_{\pi q} - \sqrt{\lambda_\pi \lambda_q}} \right] + \ln \left[ \frac{f_{\pi q} + \sqrt{\lambda_\pi \lambda_q}}{f_{\pi q} - \sqrt{\lambda_\pi \lambda_q}} \right] \right\} \\
& + (s \rightarrow u) \\
& + \frac{1}{16\pi \sqrt{\lambda_q} (s - m_N^2 - q^2)} \theta(q^2 - 4m_\pi^2) \\
& \times \left\{ \ln \left[ \frac{d_{\pi q} + \sqrt{\lambda_{\pi q} \lambda_q}}{d_{\pi q} - \sqrt{\lambda_{\pi q} \lambda_q}} \right] + \ln \left[ \frac{m_\pi^2 q^2 + \sqrt{\lambda_q \lambda_{\pi q}}}{m_\pi^2 q^2 - \sqrt{\lambda_q \lambda_{\pi q}}} \right] \right\}
\end{aligned}$$

with

$$\begin{aligned}
a_{\pi q} &= (s - m_N^2 + q^2)(s + m_N^2 - m_\pi^2) - 2sq^2 \\
b_{\pi q} &= (s + m_N^2 - q^2)(s + m_N^2 - m_\pi^2) - 2s(2m_N^2 - m_\pi^2) \\
c_{\pi q} &= q^2(s - m_N^2 - q^2 + 2m_\pi^2) \\
d_{\pi q} &= q^2(s - m_N^2 - q^2 - m_\pi^2) \\
e_{\pi q} &= (s - m_N^2 + q^2)(s - m_N^2 + m_\pi^2) - 2sq^2 \\
f_{\pi q} &= 2s(s - m_N^2) - (s - m_N^2 + q^2)(s - m_N^2 + m_\pi^2).
\end{aligned}$$

These imaginary parts reduce to those in [19] for  $q^2 = 0$ . Increasing  $q^2$  leads to  $\lambda_q$  becoming negative and the analytically continued forms of the above expressions, for example

$$\text{Im } \Gamma^{\pi N}(s) = -\frac{1}{8\pi \sqrt{-\lambda_q}} \arctan \left( \frac{\sqrt{\lambda_\pi \lambda_q}}{a_{\pi q}} \right) \theta(s - s_0),$$

must be used.

## Appendix C

We use the following conventions for the  $\Delta$ 's sum over spins and propagator

$$\begin{aligned}
\sum_s u_\mu^i(p) \bar{u}_\nu^j(p) &= \left( \delta^{ij} - \frac{\tau^i \tau^j}{3} \right) \frac{\not{p} + m_\Delta}{2m_\Delta} P_{\mu\nu}(p) \\
\Delta_{\mu\nu}^{ij}(p) &= \left( \delta^{ij} - \frac{\tau^i \tau^j}{3} \right) \frac{i(\not{p} + m_\Delta)}{p^2 - m_\Delta^2 + im_\Delta \Gamma_\Delta} P_{\mu\nu}(p)
\end{aligned}$$

with

$$P_{\mu\nu}(p) = g_{\mu\nu} - \frac{1}{3}\gamma_\mu \gamma_\nu - \frac{1}{3m_\Delta} \gamma_{[\mu} p_{\nu]} - \frac{2}{3m_\Delta^2} p_\mu p_\nu.$$

Defining  $(\nu, \nu_p, \nu_q) = (p \cdot q, k \cdot p, k \cdot q)/m_N$  and  $k^2 = s$ , we find

$$\begin{aligned}
\sum_{s, I} |\langle N(p) | \mathbf{V}_\mu^3 | \Delta(k) \rangle|^2 &\equiv \mathcal{M}(s, q^2) \\
&\equiv \frac{8}{9m_\Delta} \left[ 2m_N \nu_q^2 \mathcal{M}_1(s, q^2) + 2m_N \nu_q^2 q^2 \mathcal{M}_2(s, q^2) \right. \\
&\quad \left. + q^2 \mathcal{M}_3(s, q^2) + q^4 \mathcal{M}_4(s, q^2) + q^6 \mathcal{M}_5(s, q^2) \right]
\end{aligned}$$

$$\begin{aligned}
\mathcal{M}_1(s, q^2) &= \left( \frac{\nu}{\nu_q} + \frac{\nu_p r^2}{m_N} \right) Q^2 + 2r^2 \nu_q \nu S^2 \\
&\quad - 2r(2\nu - r\nu_q) Q S \\
\mathcal{M}_2(s, q^2) &= \left( \frac{5\nu}{\nu_q} - 2r - \frac{\nu}{\nu_q} \frac{s}{m_\Delta^2} \right) Q \bar{R} \\
&\quad + \frac{r}{2m_\Delta} (\nu_p - m_\Delta) R^2 - r(r\nu_q + \nu) \bar{R} S \\
&\quad + r(r\nu_q - \nu) R \bar{R} + r^2 \nu_q \nu \bar{R}^2 \\
&\quad + \left( \frac{\nu}{\nu_q} \left( 1 + \frac{s}{m_\Delta^2} \right) - \frac{r}{m_\Delta} (\nu_p + m_\Delta) \right) R S \\
&\quad + \left( \frac{3r}{2} - \frac{2\nu}{\nu_q} - \frac{r\nu_p}{2m_\Delta} \right) S^2 \\
\mathcal{M}_3(s, q^2) &= \left( \nu_p \left( \frac{s}{m_\Delta^2} - 2 \right) - 3m_\Delta \right) Q^2 \\
&\quad + m_\Delta \nu_q \left( \frac{\nu}{\nu_q} \left( \frac{s}{m_\Delta^2} - 2 \right) + 5r - \frac{4r}{m_\Delta} \nu_p \right) Q R \\
&\quad + m_\Delta \nu_q \left( \frac{\nu}{\nu_q} \left( 9 - \frac{s}{m_\Delta^2} \right) - 6r + \frac{2s}{m_\Delta^2} r \right) Q S \\
\mathcal{M}_4(s, q^2) &= \left( \frac{s}{m_\Delta} - 4\nu_p - 3m_\Delta + \frac{2s}{m_\Delta^2} \nu_p \right) Q \bar{R} \\
&\quad + (\nu_p - m_\Delta) \left( 3 - \frac{s}{m_\Delta^2} \right) R^2 \\
&\quad + (m_N \nu_q - m_\Delta \nu) \left( 5 - \frac{2s}{m_\Delta^2} \right) R \bar{R} \\
&\quad + \left( 3m_\Delta - 2\nu_p - \frac{s}{m_\Delta} \right) R S \\
&\quad + \nu_q \nu \left( 6m_N - \frac{2s}{m_\Delta} r - \frac{\nu_q}{\nu} (m_\Delta + \nu_p) r^2 \right) \bar{R}^2 \\
&\quad + \left( 3m_\Delta \nu + \frac{s}{m_\Delta^2} (2m_N \nu_q - m_\Delta \nu) \right) \bar{R} S \\
&\quad + (\nu_p - 3m_\Delta) S^2 \\
\mathcal{M}_5(s, q^2) &= - \left( 3 - \frac{s}{m_\Delta^2} \right) (m_\Delta + \nu_p) \bar{R}^2
\end{aligned}$$

with  $r = m_N/m_\Delta$  and the sum over spins including the photon, nucleon, and the  $\Delta$ .

## Appendix D

We quote here the full on-shell Ward-identity for  $\mathbf{W}_{\pi\pi}^F$ . It contains the  $\pi\pi$  forward scattering amplitude  $i\mathcal{T}_{\pi\pi}$  and the pion-spin averaged  $\pi\gamma$  scattering amplitude  $i\mathcal{T}_{\pi\gamma}$  both quoted in [11].

$$\begin{aligned}
\frac{1}{f_\pi^4} \mathbf{W}_{\pi\pi}^F(q, k_1, k_2) &= \\
&= -(2k_1 + q)^2 \sum_{a,b} \epsilon^{a3e} \epsilon^{a3f} \text{Im } \mathcal{T}_{\pi\pi}^{be \rightarrow bf} ((k_1 + q), k_2) \\
&\quad + (q \rightarrow -q) \\
&\quad + \frac{2}{f_\pi^2} (g_{\mu\nu} - (2k_1 + q)_\mu k_{1\nu} \Delta_R(k_1 + q)) \text{Im } \mathcal{T}_{\pi\gamma}^{\mu\nu}(q, k_2)
\end{aligned}$$

$$\begin{aligned}
&+ (q \rightarrow -q) + (k_1 \rightarrow -k_1) + (q, k_1 \rightarrow -q, -k_1) \\
&+ \frac{1}{f_\pi} k_1^\alpha (2k_1 + q)^\mu \sum_a \epsilon^{a3e} \text{Im } \mathcal{A}_{\alpha\mu}^{ae}(k_1, q) \\
&+ (q \rightarrow -q) + (k_1 \rightarrow -k_1) + (q, k_1 \rightarrow -q, -k_1) \\
&+ \text{Im } \sum_b \frac{3m_\pi^2}{f_\pi^2} \int d^4x d^4y e^{iq \cdot (x-y)} \\
&\times \langle \pi_{\text{out}}^b(k_2) | T^* \mathbf{V}_\mu^3(x) \mathbf{V}^{3,\mu}(y) \hat{\sigma}(0) | \pi_{\text{in}}^b(k_2) \rangle \\
&- \frac{1}{f_\pi^2} \sum_a \epsilon^{a3e} \epsilon^{e3g} (2k_1 + q)^\mu k_1^\alpha \Delta_R(k_1 + q) \text{Im } \mathcal{B}_{\alpha\mu}^{ag}(k_1, k_2) \\
&- \frac{1}{f_\pi^2} (g^{\mu\nu} - (k_1 + q)^\mu (2k_1 + q)^\nu \Delta_R(k_1 + q)) \\
&\times \sum_a \epsilon^{a3e} \epsilon^{a3f} \text{Im } \mathcal{B}_{\mu\nu}^{ef}(k_1 + q, k_2) \\
&- \frac{1}{f_\pi^2} k_1^\alpha k_1^\beta \Delta_R(k_1) \sum_a \epsilon^{a3e} \epsilon^{g3e} \text{Im } \mathcal{B}_{\alpha\beta}^{ag}(k_1, k_2) \\
&+ \frac{1}{f_\pi^2} k_1^\alpha k_1^\beta (2k_1 + q)^2 \Delta_R(k_1 + q) \Delta_R(k_1) \\
&\times \sum_a \epsilon^{a3e} \epsilon^{g3e} \text{Im } \mathcal{B}_{\alpha\beta}^{ag}(k_1, k_2) \\
&+ (q \rightarrow -q) + (k_1 \rightarrow -k_1) + (q, k_1 \rightarrow -q, -k_1) \\
&- \frac{1}{f_\pi^2} (k_1 + q)^\alpha (k_1 + q)^\beta (2k_1 + q)^2 \Delta_R^2(k_1 + q) \\
&\times \sum_a \epsilon^{a3e} \epsilon^{a3f} \text{Im } \mathcal{B}_{\alpha\beta}^{ef}(k_1, k_2) + (k_1 \rightarrow -k_1) \\
&- \frac{1}{f_\pi^2} g^{\mu\nu} k_1^\alpha \sum_a \epsilon^{a3e} \text{Im } i\mathcal{C}_{\mu\nu\alpha}^{ea}(q, k_1 + q, k_1) + (k_1 \rightarrow -k_1) \\
&+ \text{Im } \frac{1}{f_\pi^2} (2k_1 + q)^\mu (k_1 + q)^\alpha k_1^\beta \Delta_R(k_1 + q) \\
&\times \sum_a \epsilon^{a3e} i\mathcal{C}_{\mu\nu\alpha}^{ea}(q, k_1 + q, k_1) \\
&- \frac{1}{f_\pi^2} k_1^\alpha k_1^\beta \int d^4x d^4y d^4z e^{ik_1 \cdot (y-x)} e^{iq \cdot z} \\
&\times \text{Im } i \langle \pi_{\text{out}}^b(k_2) | T^* \mathbf{j}_{A\alpha}^a(x) \mathbf{j}_{A\beta}^a(y) \mathbf{V}_\mu^3(z) \mathbf{V}^{3,\mu}(0) | \pi_{\text{in}}^b(k_2) \rangle
\end{aligned}$$

with

$$\begin{aligned}
\mathcal{A}_{\alpha\mu}^{ae}(k_1, q) &\equiv \sum_b \int d^4x d^4y e^{ik_1 \cdot x} e^{iq \cdot y} \\
&\times \text{Im } \langle \pi_{\text{out}}^b(k_2) | T^* (\mathbf{j}_{A\alpha}^a(x) \mathbf{V}_\mu^3(y)) \pi_{\text{in}}^b(0) | \pi_{\text{in}}^b(k_2) \rangle \\
&= \frac{1}{f_\pi} \delta^{ae} (2k_1 + q)_\alpha \int d^4x e^{ik_1 \cdot x} \\
&\times \text{Im } \langle \pi_{\text{out}}^b(k_2) | T^* \mathbf{V}_\mu^3(x) \hat{\sigma}(0) | \pi_{\text{in}}^b(k_2) \rangle \\
&+ \text{Im } \frac{1}{f_\pi} \epsilon^{e3g} (2k_1 + q)_\mu k_1^\beta \Delta_R(k_1) \mathcal{B}_{\alpha\beta}^{ag}(k_1, k_2) \\
&+ \frac{1}{f_\pi} \epsilon^{e3g} (\delta_\mu^\beta - (2k_1 + q)_\mu k_1^\beta) \text{Im } \mathcal{B}_{\alpha\beta}^{ag}(k_1, k_2) \\
&- \frac{1}{f_\pi} (k_1 + q)^\beta \int d^4x d^4y e^{iq \cdot x} e^{ik_1 \cdot y} \\
&\times \text{Im } i \langle \pi_{\text{out}}^b(k_2) | T^* \mathbf{V}_\mu^3(x) \mathbf{j}_{A\alpha}^a(y) \mathbf{j}_{A\beta}^a(0) | \pi_{\text{in}}^b(k_2) \rangle
\end{aligned}$$

$$\begin{aligned}
& + \frac{1}{f_\pi} \epsilon^{age} \int d^4x e^{iq \cdot x} \\
& \times \text{Im} i \langle \pi_{\text{out}}^b(k_2) | T^* \mathbf{V}_\mu^3(x) \mathbf{V}_\alpha^g(0) | \pi_{\text{in}}^b(k_2) \rangle \\
\mathcal{B}_{\alpha\mu}^{ag}(k_1, k_2) & \equiv \\
= i \sum_b & \int d^4x e^{ik_1 \cdot x} \langle \pi_{\text{out}}^b(k_2) | T^* \mathbf{j}_{A\alpha}^a(x) \mathbf{j}_{A\mu}^g(0) | \pi_{\text{in}}^b(k_2) \rangle \\
\mathcal{C}_{\mu\nu\alpha}^{ea}(q, k_1 + q, k_1) & \equiv \\
= \sum_b & \int d^4x d^4y e^{i(k_1+q) \cdot x} e^{-ik_1 \cdot y} \\
& \times \langle \pi_{\text{out}}^b(k_2) | T^* \mathbf{V}_\mu^3(0) \mathbf{j}_{A\nu}^e(x) \mathbf{j}_{A\alpha}^a(y) | \pi_{\text{in}}^b(k_2) \rangle
\end{aligned}$$

- 
- [1] G. Agakichiev, *et al.*, Phys. Rev. Lett. 75 (1995) 1272; Nucl. Phys. A610 (1996) 317c.
- [2] M. Masera for the HELIOS-3 Collaboration, Nucl. Phys. A590 (1995) 93c.
- [3] R. Santo *et al.*, Nucl. Phys. A566 (1994) 61c; R. Albrecht *et al.*, Nucl. Phys. A590 (1995) 81c.
- [4] E.V. Shuryak Phys. Lett. B79 (1978) 135; L.D. McLerran and T. Toimela, Phys. Rev. D31 (1985) 545; K. Kajantie, J. Kapusta, L. McLerran, and A. Mekjian, Phys. Rev. D34 (1986) 2476; E. Braaten, R.D. Pisarski, and T.C. Yuan, Phys. Rev. Lett. 64 (1990) 2242; H.A. Weldon, Phys. Rev. Lett. 66 (1991) 293; J. Kapusta, P. Lichard, and D. Seibert, Phys. Rev. D44 (1991) 2774; L. Xiong, E.V. Shuryak, and G.E. Brown, Phys. Rev. D46 (1992) 3798; C. Gale and P. Lichard, Phys. Rep. D49 (1994) 3338; D. Srivastava and B. Sinha, Phys. Rev. Lett. 73 (1994) 2421; Z. Huang, Phys. Lett. B361 (1995) 131; W. Cassing, W. Ehehalf, and C.M. Ko, Phys. Lett. B363 (1995) 35; R. Baier, M. Dirks and K. Redlich, hep-ph/9612448.
- [5] G.Q. Li, C.M. Ko, and G.E. Brown, Nucl. Phys. A606 (1996) 568.
- [6] C.M. Hung and E.V. Shuryak, to be published in Phys. Rev. C, hep-ph/9608299.
- [7] T. Hatsuda, nucl-th/9608037.
- [8] R. Rapp, G. Chanfray, and J. Wambach, to be published in Nucl. Phys. A, hep-ph/9702210.
- [9] F. Klingl and W. Weise, Nucl. Phys. A606 (1996) 329; F. Klingl, N. Kaiser, and W. Weise, hep-ph/9704398.
- [10] J.V. Steele, H. Yamagishi, and I. Zahed, Phys. Lett. B384 (1996) 255.
- [11] H. Yamagishi and I. Zahed, Ann. Phys. 247 (1996) 292.
- [12] J. Sollfrank, P. Huovinen, M. Kataja, P.V. Ruuskanen, M. Prakash, and R. Venugopalan, Phys. Rev. C55 (1997) 392.
- [13] J.V. Steele, H. Yamagishi, and I. Zahed, to be published.

- [14] J.V. Steele, H. Yamagishi, and I. Zahed, Nucl. Phys. A615 (1997) 305; J.V. Steele, H. Yamagishi, and I. Zahed, hep-ph/9512233; S. Chernyshev and I. Zahed, hep-ph/9511271.
- [15] L.D. McLerran and T. Toimela, Phys. Rev. D31 (1985) 545; H.A. Weldon, Phys. Rev. D42 (1990) 2384.
- [16] H.A. Weldon, Ann. Phys. 228 (1993) 43.
- [17] "Total Cross Sections for Reactions of High Energy Particles", Landolt-Börnstein, New Series Vol. I/12a and I/12b, ed. H. Schopper (1988).
- [18] Particle Data Group, Phys. Rev. D50 (1994) 1341.
- [19] V. Bernard, N. Kaiser, and U.-G. Meissner, Nucl. Phys. B373 (1992) 346.
- [20] H.F. Jones and M.D. Scadron, Ann. Phys. 81 (1973) 1; M. Benmerrouche, R.M. Davidson and N.C. Mukhopadhyay, Phys. Rev. C39 (1989) 2339; R.M. Davidson, N.C. Mukhopadhyay, and R.S. Wittman, Phys. Rev. D43 (1991) 71.
- [21] M. Schafer, H.C. Donges, A. Engel, and U. Mosel, Nucl. Phys. A575 (1994) 429.
- [22] H. Sorge, Phys. Lett. B373 (1996) 16.
- [23] R. Rapp, private communication.
- [24] M. Kacir and I. Zahed, Phys. Rev. D54 (1996) 5536.
- [25] H. Herrmann, B.C. Friman, and W. Norenberg, Nucl. Phys. A560 (1993) 411.